Emissivity of Sea Ice at 89 GHz, 157 GHz and 183 GHz in the Arctic winter

Nathalie A. Selbach, Tim J. Hewison, *Member, IEEE,* and Georg Heygster, *Member, IEEE*

***Abstract*— Satellite remote sensing can provide valuable data on atmospheric parameters in data sparse polar areas. Currently, the use of satellite data in these regions is restricted due to the high and variable surface emissivity. A method to determine the surface emissivities at 89 GHz, 157 GHz and 183 GHz of different types of sea ice is presented. Additionally, a method has been developed to calculate an effective surface temperature from the three channels near 183 GHz. Spectra of emissivity for different ice types over-flown during the airborne SEPOR-POLEX campaign in the Arctic in March 2001 show a general decrease in emissivity from young ice towards old ice for the three frequencies. Generally, the emissivity decreases from 89 GHz to 157 GHz and increases again at 183 GHz. A clear relationship is found between the surface emissivities at 157 GHz and 183 GHz, but not between the emissivities at 89 GHz and 157 GHz or 183 GHz, respectively. Generally, the emissivities at 89 GHz show a much higher variability than the ones at the two higher frequencies.**

***Index Terms*— Emissivity, Surface, Microwave, Millimeter Wave, Sea Ice, Arctic**

I. Introduction

RECENT studies in atmospheric and oceanic circulation have shown that polar regions play an important role in the global climate variability and change. Therefore, there is an increasing interest in these regions [1]. However, due to the remoteness of these areas and their demanding climate, direct measurements of many useful geophysical parameters are very sparse [2], [3]. Most in-situ observations are located in the coastal areas surrounding the Arctic ocean and only very few observations are available in the central Arctic. Instrumented aircraft can perform measurements in the central Arctic as well, but they do not cover the complete area and are mostly case studies. Satellite microwave radiometry, due to its good spatial and temporal coverage, potentially provides a valuable tool for global observations of atmospheric parameters like total water vapor and cloud liquid water. Difficulties arise from the large and highly changeable surface emissivity at microwave bands from the ice/snow covered surface together with the very low water vapor burden in polar regions.

Only few measurements of the surface emissivity over sea ice and snow are available in the frequency range from 89 GHz to 183 GHz. Studies on the surface emissivity over land surfaces at SSM/I frequencies (19.35 GHz to 85.5 GHz) have been performed, e.g., by [4], [5]. Surface emissivities over various surfaces at the frequencies of SSM/T2 (91 GHz to 183.3 GHz) are given in [6]. The surface emissivity in the frequency range of 24 GHz to 157 GHz over Baltic sea ice and snow sites from airborne instruments have been presented by [7]. However, measurements over snow and sea ice in the Arctic, especially at 183 GHz, are rare. The emissivity of sea ice from airborne passive microwave measurements at 37 GHz, 89/90 GHz, 150 GHz and 220 GHz near the SHEBA ice camp are given in [8]. Several studies have been performed to retrieve the emissivity of freshwater surfaces at 89 GHz, 150 GHz and 220 GHz. The analysis had been restricted to very dry conditions in order to correct for the atmospheric influence in the retrieval [9], [10]. Emissivities of snow-covered surfaces are given in [11]. However, all the above mentioned studies did not include a retrieval of the surface emissivity at 183 GHz, where the key humidity sounding channels are centered. A better understanding of the behavior of the emissivity of sea ice with or without snow cover is required to improve the estimation of atmospheric parameters in polar regions. The measurements of the SEPOR-POLEX (Surface Emissivities in Polar Regions - Polar Experiment) campaign provide a new data set of surface emissivities including measurements at 183 GHz over different types of sea ice.

N. A. Selbach is with the Institute of Environmental Physics, University of Bremen, Germany, email: nselbach@uni-bremen.de

T. J. Hewison is with the Met Office, UK, email: tim.hewison@metoffice.com

G. Heygster is with the Institute of Environmental Physics, University of Bremen, Germany, email: heygster@uni-bremen.de

II. Data

The airborne SEPOR-POLEX campaign based in Tromsø ($69°41'$ N, $18°55'$ E) in Norway took place from 8th to 29th of March. Five flights of up to 10 hours duration were performed over various ice types including new, glacier, first- and multi-year ice. Each flight consisted of a long low-level run at between 150 m to 1200 m above sea level. At the end of this run a profile ascent has been flown up to about 8.5 km above sea level, followed by a run back to the base at high level along the same track as the low level run. A northerly or north-easterly surface air flow over the ice during all flights resulted in mainly clear skies over the ice but rapid cloud development over open water in the marginal ice zone (MIZ). Two flights concentrated on measurements of the MIZ to collect data over a range of varying ice concentrations and different forms of young and new ice as well as first-year (FY) ice. The remaining three flights consisted of long runs up to 85° N at different longitudes (30° E, 0° E, 30° W). The ice was generally quite uniform with ice thickness increasing to the North. The flights are described in more detail in [12].

The key instrument for this experiment operated on the Met Office C-130 research aircraft was the passive microwave

radiometer MARSS (Microwave Airborne Radiometer Scanning System) with frequencies close to those of SSM/T2 and AMSU-B (Advanced Microwave Sounding Unit-B) [13], [14]. The airborne microwave radiometer MARSS has two channels in the atmospheric windows at 89 GHz and 157 GHz and three channels centered at the strong water vapor absorption line at 183.31 GHz. It is a total power radiometer with a 3 s along-track scan and an integration time of 100 ms for all five channels. The scan geometry allows measurements both in upward and downward direction at different angles. The performance of the instrument during the experiment is given in [12], [15]. The analysis of the data concentrates on the nominal nadir viewing direction. A broad range of meteorological and navigational instruments were operated aboard the aircraft including measurements of air temperature, humidity, pressure and wind velocity, GPS position, radar altitude and surface temperature from a thermal infrared (IR) radiometer. Further details are given in [12]. No in-situ data of snow cover, snow depth, grain size or ice thickness is available for the time period of the campaign. Observers' logs and information from a downward- and forward-facing video camera are available.

The analysis of the emissivities concentrated on the direct nadir viewing geometry. Data from different viewing angles is available for the five flights over the sea ice, which would show the viewing angle dependence of the emissivities.

III. EMISSIVITIES

A. Definition of emissivity

Before presenting the calculation of the surface emissivity ε_s, it is important to carefully define its meaning to avoid ambiguities. Here, the surface is assumed to be purely specular. This is consistent with the treatment of the sea surface in many emissivity models. However, most of the snow and ice surfaces are close to Lambertian. Furthermore, the surface is neither (vertically) homogeneous nor isothermal. The net emission is a weighted average of the emission and scattering within the surface layer contributing to the signal.

The atmosphere below the aircraft has been assumed to be vertically homogeneous. Atmospheric scattering is neglected in this study as no clouds have been allowed below the aircraft for the surface observations. The brightness temperature T_n (Fig. 1) received at the downward looking radiometer in height h can be written as follows:

$$T_\mathrm{n} = T_\mathrm{a} + \varepsilon_\mathrm{s} T_\mathrm{s} \exp(-\tau) + (1-\varepsilon_\mathrm{s}) T_\mathrm{d} \exp(-\tau) \qquad (1)$$

The first term in (1), T_a, describes the upwelling atmospheric emission. The contribution of the surface is described in the second term by its temperature T_s and emissivity ε_s and affected by absorption in the layer between the surface and aircraft level. The third term is the downwelling atmospheric radiation which is reflected at the surface and affected by absorption in the layer below the aircraft, given by the term $\exp(-\tau)$. Assuming an isothermal layer with a mean temperature T_m and an opacity τ, T_a can be calculated as

$$T_\mathrm{a} = (1 - \exp(-\tau)) T_\mathrm{m} \qquad (2)$$

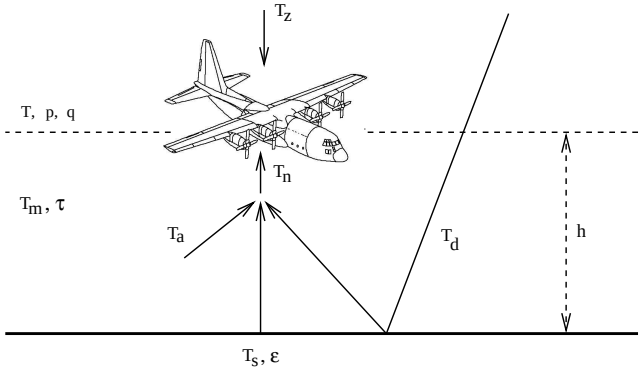

Fig. 1. Systematic sketch of the different contributions of the signal measured at the downward looking radiometer

The downwelling radiation is measured at the upward looking radiometer at height h (T_z in Fig. 1). The downwelling atmospheric radiation below the aircraft is expressed as in (2). The part of the radiation measured at height h has to be corrected for the absorption in the layer below the aircraft resulting in

$$T_\mathrm{d} = T_\mathrm{z} \exp(-\tau) + T_\mathrm{a} \qquad (3)$$

Rewriting (1) gives an expression for the surface emissivity:

$$\varepsilon_\mathrm{s} = \frac{T_\mathrm{n} - T_\mathrm{a} - T_\mathrm{d} \exp(-\tau)}{(T_\mathrm{s} - T_\mathrm{d}) \exp(-\tau)} \qquad (4)$$

T_n and T_z are directly measured at the height h above the surface. The atmospheric absorption and the mean temperature of the layer are modeled with the help of additional aircraft data [12], [16]. Thus, the only unknown in (4) is the surface temperature T_s. The uncertainty in the calculation of ε_s is dominated by the uncertainty in the atmospheric correction. The uncertainty in water vapor in the layer below the aircraft is the main source of errors.

B. Surface Temperature

The emissivity calculated according to (4) depends strongly on the definition of T_s. One possibility is the use of a surface skin temperature derived from an infrared radiometer as used in [7]. However, microwaves penetrate some depth into snow and sea ice. Due to the typical temperature structure in sea ice and dry snow in winter, the effective emitting temperature is higher than the surface skin temperature. To overcome the difference in penetration depth in the IR and microwave range of the electromagnetic spectrum as well as for the unknown emissivity in the IR, a method has been developed to calculate an effective emitting surface temperature from the measurements of the three channels centered on the water vapor absorption line. The surface emissivity is assumed to be the same for the three channels. The effective surface temperature T_eff is calculated by minimizing a cost function F_c with respect to the surface temperature. The cost function is defined as the sum over the squared differences between the observed nadir brightness temperatures ($T_\mathrm{n}{}^{OBS}$) and those

from the radiative transfer equation ($T_{\mathrm{n}}{}^{RTE}$):

$$F_c = \sum_i (T_{n,i}^{OBS} - T_{n,i}^{RTE})^2 \qquad i = 1, 2, 3 \qquad (5)$$

where i is the number of the channels centered at the water vapor absorption line at 183 GHz. $T_{n,i}^{RTE}$ is the brightness temperature, given by (1) using (2) and (3) to obtain T_a and T_d [12]. The resulting effective temperature is used as input in (4) to calculate ε_s. The penetration depth at 89 GHz and 157 GHz is greater than at 183 GHz. Due to the increase in temperature within the snow and ice pack during winter, the effective emitting temperature for these channels was higher than the temperature retrieved from the measurements at 183 GHz. This leads to an underestimation of the surface emissivity for these channels as can be seen from (4). Nevertheless, this effective temperature was much closer to the real effective temperature than the skin temperature retrieved from IR measurements.

Assuming the surface to be a blackbody in the IR, typical differences between the effective temperature calculated using the above proposed method and the IR skin temperature from a Heimann IR radiometer were in the order of 12 K over the compact thick sea ice. Typical differences for young ice types were in the order of 5 K to 7 K. The thermal conductivity of snow is about an order of magnitude lower than the one of sea ice [17]. Due to a lack of information on the thickness of the snow and ice cover or the temperature profile within the snow pack a quantitative interpretation of the magnitude of the difference between these two temperatures is not possible for this study.

The proposed method is insensitive to scattering by small atmospheric ice crystals often found in the surface inversions (e.g., [18]), which is difficult to correct for in the IR measurements.

C. Results

Fig. 2 shows an example of emissivities at 89 GHz, 157 GHz and 183 GHz for an area of FY ice. The mean emissivity for each frequency and one standard deviation are shown for the time period given in the title of the figure. The flight took place on 20 March, 2001. It comprises data of about 230 km along the flight track. The data shown here covers the flight track from about 82.2° N, 2° E to 83.8° N, 3° W. Additionally, a histogram of the data is shown to the right for each frequency showing the variability of the obtained values. The bin size in the histogram is 0.001. Homogeneous areas have been selected from the video tapes. However, the inspection by eye is not always clear and sometimes results in misclassifications. In the presence of snow cover, it is difficult to give information on the underlying surface type. The mean emissivity and standard deviation of the emissivities are given in Table I.

The emissivity decreases from 89 GHz to 157 GHz and increases again at 183 GHz. A similar behavior has been reported by [8] for frequencies at 89 GHz, 150 GHz and 220 GHz. Fig. 2 shows a higher variability in the emissivity at 89 GHz compared to the values at 157 GHz and 183 GHz. In general, the penetration depth in snow and sea ice is higher at lower frequencies. Thus, the signal received at 89 GHz results from

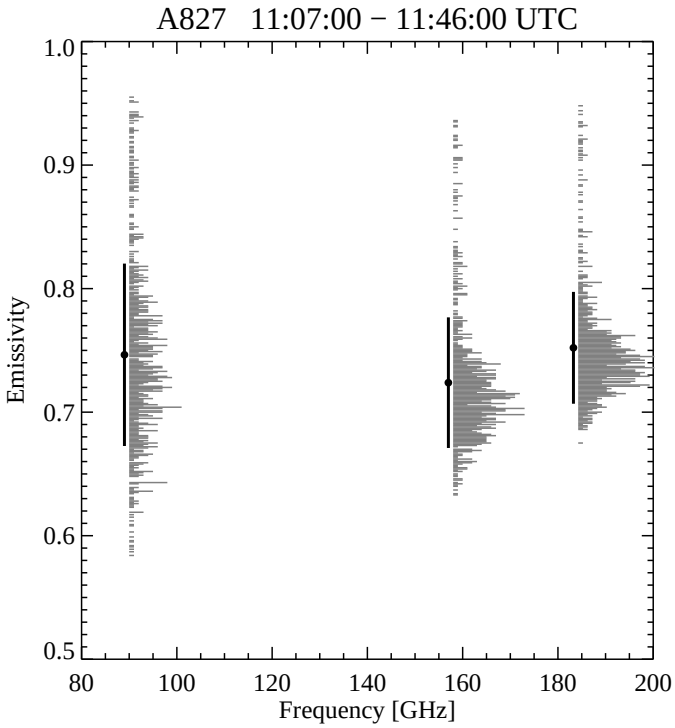

Fig. 2. Spectrum of surface emissivity for FY ice. The mean emissivity and one standard deviation are shown. Additionally a histogram of the data for the given time period is shown in gray for each frequency. The data shown here covers the flight track from about 82.2 ° N, 2° E to 83.8° N, 3° W overflown on 20 March, 2001.

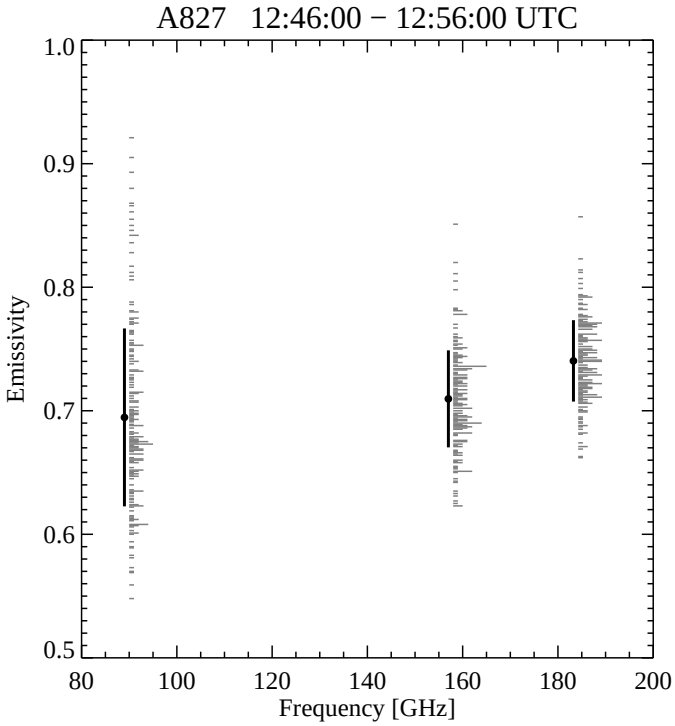

Fig. 3. Spectrum of surface emissivity for MY ice. The same parameters as in Fig. 2 are shown.The data shown here covers the flight track from about 85.0° N, 30.8° W to 85.0° N, 36.1° W overflown on 20 March, 2001.

TABLE I
MEAN EMISSIVITY (MEAN) AND STANDARD DEVIATION (STDDEV) AT 89 GHZ, 157 GHZ AND 183 GHZ FOR THE GIVEN SAMPLES

Ice type	89 GHz		157 GHz		183 GHz	
	Mean	Stddev	Mean	Stddev	Mean	Stddev
Open Water	0.638	0.005	0.712	0.005	0.732	0.007
Nilas	0.956	0.008	0.922	0.015	0.919	0.016
Pancake	0.869	0.027	0.866	0.023	0.873	0.022
FY ice, flat	0.819	0.043	0.733	0.036	0.763	0.032
FY ice, ridged	0.746	0.074	0.724	0.053	0.752	0.045
MY ice	0.695	0.072	0.709	0.039	0.740	0.033

layers deeper in the snow and sea ice than for the channels at 183 GHz and, therefore, gets signals from layers which contribute less or not at all to the signal of the higher frequencies. This explains the higher variability of the emissivities at 89 GHz. Also the greater contrast in emissivity between open water and pure ice at 89 GHz will give more variability. Some very high surface emissivities, larger than 0.9, have been calculated from the given data set. These values are typical for young ice (Fig. 4). Most probably areas of young ice, which have been covered by snow, have been over-flown. As an identification of the ice type below the snow cover is not possible from visual inspection, these measurements are included in the sample of FY ice.

Part of the signal results from the snow layer and not only from the sea ice. The influence of the snow layer increases towards higher frequencies. Due to the low surface temperatures at the time of the observation, the snow is assumed to be dry. The effect of scattering increases with frequency up to a certain point. This results in a weakening of the emission of sea ice due to an enhanced scattering by snow at higher frequencies, as the extinction by dry snow is typically dominated by scattering processes. Haggerty and Curry [8] used Mie theory to show that the scattering efficiency did not increase above 150 GHz for the conditions of their experiment. This, together with the lower penetration depth and vertical temperature gradientinfluencing the snow metamorphism , would explain the increase in emissivity above 150 GHz.

Fig. 3 shows a second example of the spectrum of emissivities for the frequencies for an area of MY ice overflown on the same day as for the sample shown in Fig. 2. The data shown here covers the flight track from about 85.0° N, 30.8° W to 85.0° N, 36.1° W. The mean emissivity for the three frequencies is generally lower than for the sample of FY ice shown in Fig. 2. The mean emissivity at 89 GHz is slightly smaller than the one at 157 GHz (Table I). As for the example of FY ice, the emissivity increases from 157 GHz towards 183 GHz. As for the sample of FY ice, the variability of the emissivity at 89 GHz is larger than for the two higher frequencies (Table I).

Fig. 4 shows the mean emissivities for several samples of different surface types observed during the SEPOR-POLEX campaign as a function of the frequency. The mean values are connected by straight lines. These straight lines do not indicate that the emissivities may be interpolated between the observation frequencies. The mean emissivity and standard deviation for the examples are given in Table I. An increase with frequency can be seen for the emissivity of open water

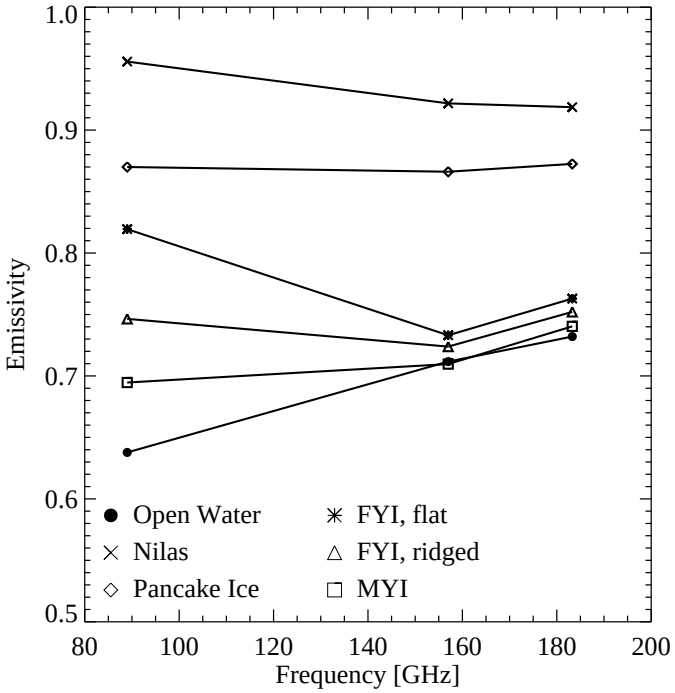

Fig. 4. Typical surface emissivity for different types of sea ice during the SEPOR-POLEX campaign

with low values. A distinction of open water and sea ice is possible at 89 GHz. The emissivity of open water at 157 GHz and 183 GHz shows an overlap with emissivities of older and thicker FY ice and especially MY ice. A general decrease of emissivity can be seen for the surface types which are dominant in the more central part of the Arctic. Younger ice as Nilas and pancake ice, having a higher percentage in the MIZ, show a high surface emissivity and only a weak dependence on frequency. Refrozen leads were quite often observed within the area of compact sea ice. Areas of younger ice types with their high surface emissivities have a large effect on the mean emissivity within the field of view of the instrument. The channel at 89 GHz shows the largest variability of values within each of the samples and also for the different types of sea ice compared to the channels at 157 GHz and 183 GHz (see Table I).

Fig. 5 and 6 show scatter plots of the emissivities at 183 GHz and 157 GHz, and 89 GHz and 157 GHz, respectively. The emissivities calculated from the runs at low level for all five flights are shown in these plots including all surface types. No averaging has been applied to the data shown in these plots. Fig. 5 shows the relation between the two higher frequencies. Generally, the emissivity at 157 GHz is lower than at 183 GHz, as has already become apparent in Fig. 4. The data show a clear linear trend of the emissivities at 157 GHz and 183 GHz. The coefficients for a linear fit and the resulting rms error are given in the figure. Thus, if the emissivity at 157 GHz is precisely known, it is possible to parameterize the emissivity at 183 GHz with an rms error of 0.018. The linear correlation coefficient is 0.981. If the surface temperature were accurately known, this would correspond to an uncertainty in brightness temperature at the top of the atmosphere of about 1.4 K for the

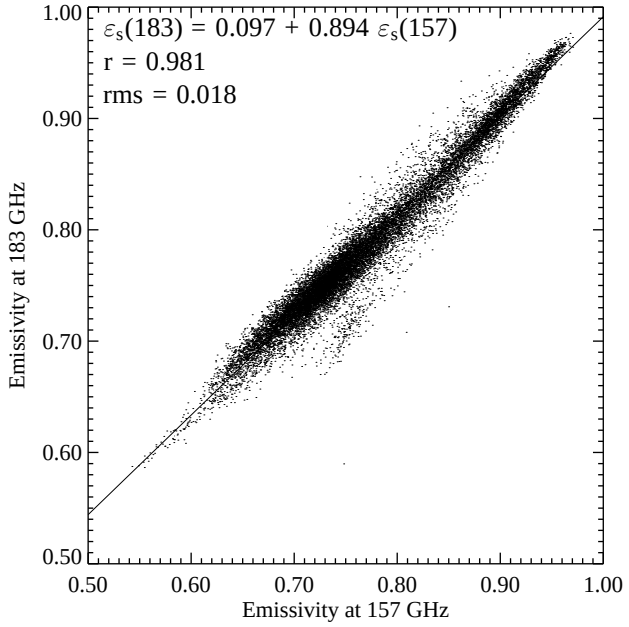

Fig. 5. Scatter plot of the emissivities at 157 GHz and 183 GHz for the data of all low-level runs during SEPOR-POLEX

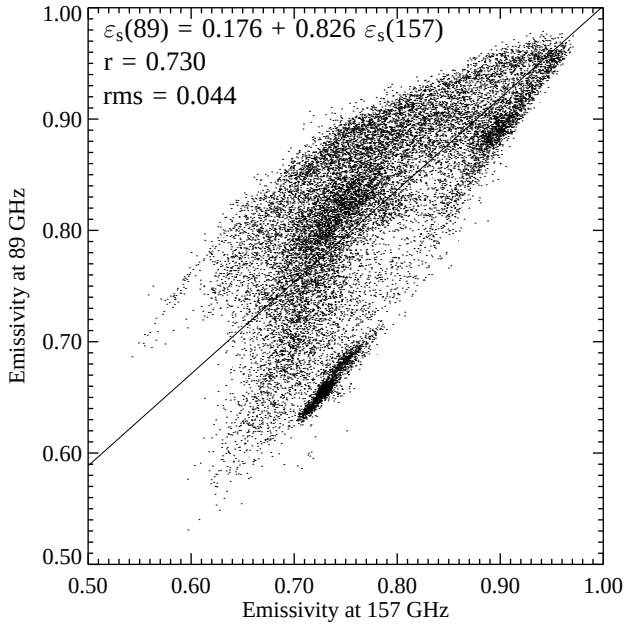

Fig. 6. Scatter plot of the emissivities at 157 GHz and 89 GHz for the data of all low-level runs during SEPOR-POLEX

channel at 183 ± 7 GHz in typical arctic winter conditions. This is an encouraging result for the analysis of satellite data over the sea ice. The effect of differences in surface emissivity on the retrieval of, e.g., atmospheric total water vapor in the polar regions can be reduced [12]. The data of the SEPOR-POLEX campaign is only a case study and the emissivities calculated in this study cannot be assumed to be representative for other areas or seasons in the Arctic.

Fig. 6 shows a similar scatter plot for the emissivities retrieved for the channels at 89 GHz and 157 GHz. As expected from Fig. 4, there is much more scatter and, compared to the emissivities at 157 GHz and 183 GHz, there is no clear trend, but areas of open water clearly exhibit a different signature to ice. The linear correlation coefficient is 0.730 - smaller than for the case of the two higher frequencies. Similarly, estimating the emissivity at 89 GHz from precise measurements at 157 GHz would result in an rms error of 0.044. If the surface temperature is also accurately known, this corresponds to an uncertainty in a satellite's 89 GHz brightness temperature of about 8.3 K typically. The cluster of low emissivities can be attributed to open water. There is less variability for higher emissivities than for the lower range of emissivities. High emissivities are typical for younger ice types. These only have a weak dependence on frequency and show less variability than the examples of FY ice. The much higher variability of the emissivities shows the general difficulty of accounting for the emissivity in the retrieval of atmospheric parameters over the sea ice in this frequency range.

IV. Conclusions

A method has been developed to retrieve the emissivity at 89 GHz, 157 GHz and 183 GHz of sea ice from low-level flight during SEPOR-POLEX, accounting for atmospheric effects below the aircraft. An effective surface temperature has been used which accounts for the penetration of the signal into the sea ice and snow pack. The effective surface temperature can be calculated from the measurements of three channels centered at the water vapor absorption line at 183 GHz.

The emissivity of the sea ice varies with frequency but also within an apparently homogeneous area. The effect of snow on the sea ice is difficult to estimate from the available data. For all three frequencies a decrease in emissivity is seen from young towards old (MY) ice. In general, a decrease in emissivity is seen from 89 GHz to 157 GHz, while the emissivity is typically larger at 183 GHz than at 157 GHz. A linear trend of the emissivities at 157 GHz and 183 GHz is seen in the data which is an encouraging result for the improvement of the determination of atmospheric parameters over the sea ice using these frequencies. A similar relationship is not found for the channel at 89 GHz in combination with one of the higher frequencies, suggesting different emission/scattering mechanisms are important.

These emissivities allow the surface contribution to be accounted for in the retrieval of atmospheric parameters over sea ice from satellite data. This contribution is large, due to the high surface emissivity and typically low water vapor

burden in polar regions. Accounting for the different emissivity observed at different channels improves the retrieval of total water vapor over sea ice significantly [12]. However, as the emissivities are highly variable in time and space, the application to satellite data is still difficult.

ACKNOWLEDGMENTS

SEPOR was funded under the Framework Programme V – Improving the Human Research Potential and Socio Economic Knowledge Base under the Transnational Access to major Research Infrastructures from the CAATER programme, contract no. HPRI-CT-1999-00095. This work was partly supported by the EU-funded project IOMASA (Integrated Observation and Modeling of Arctic Sea ice and Atmosphere, EVK3-CT-2002-00067).

REFERENCES

[1] D. H. Bromwich, "Introduction to special section: Synoptic and mesoscale weather system in the polar regions," *J. Geophys. Res.*, vol. 102, no. 13, pp. 13 727–13 729, 1997.

[2] J. C. King and J. Turner, *Antarctic Meteorology and Climatology*. Cambridge, UK: Cambridge Univ. Press, 1997, 409 pp.

[3] R. Przybylak, *The Climate of the Arctic*, ser. Atmospheric and Oceanographic Sciences Library. Dordrecht, The Netherlands: Kluwer Academic Publishers, 2003, vol. 26, 270 pp.

[4] C. Prigent, W. B. Rossow, and E. Matthews, "Microwave land surface emissivities estimated from SSM/I observations," *J. Geophys. Res.*, vol. 102, no. D18, pp. 21 867–218 980, September 1997.

[5] A. S. Jones and T. H. VonderHaar, "Retrieval of microwave surface emittance over land using coincident microwave and infrared satellite measurements," *J. Geophys. Res.*, vol. 102, no. D12, pp. 13 609–13 626, June 1997.

[6] G. W. Felde and J. D. Pickle, "Retrieval of 91 and 150 GHz earth surface emissivities," *J. Geophys. Res.*, vol. 100, no. D10, pp. 20 855–20 866, October 1995.

[7] T. J. Hewison and S. J. English, "Airborne retrievals of snow and ice surface emissivity at millimeter wavelengths," *IEEE Trans. Geosci. Remote Sensing.*, vol. 37, no. 4, pp. 1871–1879, 1999.

[8] J. A. Haggerty and J. A. Curry, "Variability of sea ice emissivity estimated from airborne passive microwave measurements during FIRE SHEBA," *J. Geophys. Res.*, vol. 106, no. D14, pp. 15 265–15 277, 2001.

[9] J. R. Wang, "A comparison of the MIR-estimated and model-calculated fresh water surface emissivities at 89, 150, and 220 GHz," *IEEE Trans. Geosci. Remote Sensing*, vol. 40, no. 6, pp. 1356– 1365, June 2002.

[10] J. R. Wang and W. Manning, "Retrievals of low integrated water vapor using MIR and SSM/T-2 measurements," *IEEE Trans. Geosci. Remote Sensing*, vol. 41, no. 3, pp. 630–639, March 2003.

[11] ——, "Near concurrent MIR, SSM/T-2, and SSM/I observations over snow-covered surfaces," *Remote Sens. Environ.*, vol. 84, no. 3, pp. 457–470, March 2003.

[12] N. Selbach, *Determination of Total Water Vapor and Surface Emissivity of Sea Ice at 89 GHz, 157 GHz and 183 GHz in the Arctic Winter*, ser. Berichte aus dem Institut für Umweltphysik. Berlin: Logos-Verlag, 2003, vol. 21.

[13] Aerojet GenCorp, "System summary report for the SSM/T2 water vapor profiling sensor hardware segment," Department of the Air Force, Azusa, California, Report, 1990.

[14] R. W. Saunders, T. J. Hewison, S. J. Stringer, and N. C. Atkinson, "The radiometric characterization of AMSU-B," *IEEE Trans. Microw. Theory and Techn.*, vol. 43, no. 4, pp. 760–771, 1995.

[15] N. Selbach, T. J. Hewison, G. Heygster, J. Miao, A. J. McGrath, and J. Taylor, "Validation of total water vapor retrieval with an airborne millimeter-wave radiometer over arctic sea ice," *Radio Sci.*, vol. 38, no. 4, p. 8061, 2003, doi: 10.1029/2002RS002669.

[16] T. J. Hewison, N. Selbach, G. Heygster, J. P. Taylor, and A. J. McGrath, "Airborne Measurements of Arctic Sea Ice, Glacier and Snow Emissivity at 24-183 GHz,," in *Proc. IGARSS 2002, 25 – 29 June, Toronto, Canada*, 2002, pp. 2851–2855.

[17] R. A. Massom, H. Eicken, C. Haas, M. O. Jeffries, M. R. Drinkwater, M. Sturm, A. P. Worby, X. R. Wu, V. I. Lytle, S. Ushio, K. Morris, P. A. Reid, S. G. Warren, and I. Allison, "Snow on antarctic sea ice," *rgeo*, vol. 39, no. 3, pp. 413–445, August 2001.

[18] J. A. Curry, W. B. Rossow, D. Randall, and J. L. Schramm, "Overview of arctic cloud and radiation characteristics," *J. Climate*, vol. 9, pp. 1731–1764, August 1996.

Nathalie A. Selbach received the Diploma degree in meteorology from the University of Bonn, Bonn, Germany, in 2000. She received the Ph.D. degree from the Department of Physics, University of Bremen, Bremen, Germany in 2003.

After working on the retrieval of atmospheric parameters from a ground-based microwave radiometer at the Institute of Meteorology, Bonn, Germany, she joined the Institute of Environmental Physics, Bremen, Germany in 2000 where she worked as a Graduate Research Assistant and received her Ph.D. degree. Her current research area is the retrieval of atmospheric water vapor and the retrieval of emissivity in polar regions from data of spaceborne and airborne microwave radiometers.

Tim J. Hewison received the B.Sc.(Hons.) degree in Physics with Astrophysics from the University of Manchester, UK in 1989 and M.Sc. in Meteorology from the University of Reading, UK in 1999.

His past work at the Met Office has included the anslysis of AMSU-B radiometric and antenna tests, the design, construction and operation of a microwave radiometer, 'Deimos' for use on a reseach aircraft, as well as planning and analysis of aircraft experiments to measure the emissivity of various surfaces and validation of radiative transfer models. He is now working on the development of ground-based remote sensing systems and assimilation of their data on temperature and humidity profiles for operational Numerical Weather Prediction.

Georg Heygster was born in Braunschweig, Germany, in 1951. He received the Diplomphysiker degree in 1976 in solid state physics and the Dr. rer. nat. degree in image processing in 1979, both from the University of Göttingen, Germany.

He was a consultant in the Computer Center of the University of Bremen from 1979 to 1988. Since then, after one year in the field of imaging mechanisms of the scanning acoustic microscope, he has been head of the group PHAROS (Physical Analysis of RemOte Sensing images), Institute of Environmental Physics, University of Bremen, Germany. His research activities include passive and active microwave remote sensing, especially of both surface and atmosphere of the high latitudes.

He was or still is principal investigator or co-investigator for a number of space experiments. Moreover, he was or currently is in charge of many research projects funded by EU, ESA, DFG, BMBF, DLR and other organizations. These projects include the development of sensor hardware and software, conducting campaigns, and also include the final data analysis from sensor data to geophysical parameters, and the interpretation and application of these results in many areas such as meteorology, climatology and oceanography.